Crystallographic phase transition within the magnetically ordered state of Ce_2Fe_{17}

A. Kreyssig,* S. Chang, Y. Janssen, J. W. Kim, S. Nandi, J. Q. Yan, L. Tan, R. J. McQueeney, P. C. Canfield, and A. I. Goldman

Ames Laboratory USDOE and Department of Physics and Astronomy, Iowa State University, Ames, Iowa 50011, USA

(Received 23 December 2006; published 10 August 2007)

X-ray diffraction experiments were performed on polycrystalline and single-crystal specimens of Ce_2Fe_{17} at temperatures between 10 and 300 K. Below $T_t=118\pm2$ K, additional weak superstructure reflections were observed in the antiferromagnetically ordered state. The superstructure can be described by a doubling of the chemical unit cell along the **c** direction in hexagonal notation with the same space group $R\bar{3}m$ as the room-temperature structure. The additional antiferromagnetic satellite reflections observed in earlier neutron diffraction experiments can be conclusively related to the appearance of this superstructure.

DOI: 10.1103/PhysRevB.76.054421 PACS number(s): 61.10.Nz, 61.12.Ld, 61.50.Ks, 75.50.Bb

I. INTRODUCTION

The magnetic states in R_2Fe_{17} compounds (R=rare earth) are mainly determined by the exchange interactions between the Fe moments,[1] where competition between antiferromagnetic and ferromagnetic interactions results in the appearance of an antiferromagnetic or ferromagnetic ground state related to the R ion's moment, anisotropy, and/or size.[2,3] The balance between these interactions seems particularly delicate for Ce_2Fe_{17}, where even slight structural or chemical changes can strongly modify the magnetic behavior.[4]

Ce_2Fe_{17} orders antiferromagnetically below the Néel temperature $T_N\sim208$ K. At $T_t\sim125$ K, a second transition is observed into a modified antiferromagnetic state.[4] Several publications have also reported a ferromagnetic state for their samples at low temperatures,[3,5,6] which, in our view, is most likely caused by small amounts of dopants in the investigated samples. This interpretation is supported by systematic studies of series of samples with doping or partial substitution of Fe by Al, Si, Mn, or H.[5,8–12] Furthermore, a Ce_2Fe_{17} sample with a ferromagnetic ground state at ambient pressure shows a transition into an antiferromagnetic order under isostatic compression at 3 kbar at T=40 K.[6,13,14] These studies indicate that the magnetic behavior is extremely sensitive to slight changes of the crystal structure either through modifications of the chemical composition or thermodynamic parameters, such as pressure. Significant magnetoelastic coupling has also been observed in the course of a study of the magnetic phase diagram where it was noticed that some phase transitions, in an applied magnetic field, were associated with dramatic changes in the shape of the sample.[7] So far, the relationship between the magnetic behavior and changes in the crystal structure in Ce_2Fe_{17} has been mainly based on analysis of lattice parameters or the volume of the crystallographic unit cell.[15] Here, we present an x-ray investigation on powder and single crystals focusing on qualitative changes in the crystal structure of Ce_2Fe_{17}.

Ce_2Fe_{17} crystallizes in the Th_2Zn_{17}-type structure with the rhombohedral space group $R\bar{3}m$ (166).[1] In the following, the hexagonal description is used. At room temperature, the lattice parameters are a=8.4890 Å and c=12.410 Å. The Ce atoms are located on the Wyckoff site 6c (0, 0, 0.3435). The Fe atoms occupy four different sites, 6c (0, 0, 0.0968), 9d (1/2, 0, 1/2), 18f (0.2905, 0, 0), and 18h (0.5015, 0.4985, 0.1550).[7] In two independent neutron diffraction investigations, satellite reflections were observed below T_N related to the antiferromagnetic structure with an incommensurate propagation vector in the hexagonal **c** direction. Below T_t, additional magnetic satellite reflections were present. Interestingly, these reflections were indexed as $(0\ 0\ 3/2)^{\pm}$ identifying them as satellites to a reference vector $(0\ 0\ 3/2)$.[16–18] The authors concluded that the incommensurate antiferromagnetic structure "is derived from a superstructure magnetic cell with a c parameter twice as large as the one of the nuclear cell."[16] However, in all scattering studies to date, no reflections at the position of the reference vector $(0\ 0\ 3/2)$ have been reported.

In the present investigation, these corresponding superstructure reflections have been observed in well-characterized Ce_2Fe_{17} samples. The superstructure reflections related to $(0\ 0\ 3/2)$ were studied as function of temperature between 10 and 300 K. Furthermore, entire reciprocal planes were measured using high-energy x rays and image-plate technology in order to identify additional superstructure reflections. This superstructure will be discussed in terms of its relation to the room-temperature structure and its interactions with the magnetic and electronic properties.

II. SAMPLE PREPARATION AND EXPERIMENTAL CONDITIONS

Ce_2Fe_{17} samples were grown by a self-flux technique.[7] Two types of samples were prepared for the present investigations. Single crystals with shiny surfaces were prepared in the same manner as the samples investigated in Ref. 7. For the x-ray powder diffraction measurements, a polycrystalline sample was prepared by grinding one single crystal into fine powder which was kept under acetone to prevent oxidation. In order to achieve a uniform x-ray path through the sample, this polycrystalline material was pressed into the hole of a 3 mm diameter copper disk that measured 1.2 mm thick. Both sides of the disk were covered with Kapton foil to keep the powder in place. For single-crystal x-ray diffraction experiments, a platelike single crystal with dimensions of $3\times2\times0.5$ mm^3 was selected and attached to a flat copper

sample holder. The same single-crystal was used in all single-crystal measurements.

For both the x-ray powder and single-crystal diffraction measurements, the samples were mounted on the cold finger of a helium closed-cycle cryostat where the temperature can be varied between 10 and 300 K. Two configurations for thermal shielding were employed in these measurements. First, three beryllium domes were used for thermal isolation. The inner dome was filled with helium gas to ensure good thermal exchange. A second dome between the inner and the outer domes provided additional heat shielding. The outer dome served as a vacuum enclosure. However, even though the elastic scattering of x rays by beryllium is weak, the strongly textured Debye-Scherrer rings were found to impair the observation of very weak reflections from the sample. Therefore, while searching for superstructure reflections, an aluminum can with Kapton windows was used. Although the sample temperature was no longer as well defined, the sample enclosure produced only a weak diffuse background. To define the sample temperature, measurements were performed in both configurations by keeping the sample in place and exchanging only the sample enclosures.

Two x-ray scattering instruments were employed. Preliminary single-crystal measurements were made on a standard four-circle diffractometer using Cu $K\alpha$ radiation from a high intensity rotating anode x-ray source, selected by a silicon (1 1 1) monochromator. The synchrotron x-ray diffraction measurements on the powder and single-crystal samples were performed using a six-circle diffractometer at the 6-ID-D station in the MU-CAT sector at the Advanced Photon Source, Argonne. The synchrotron radiation, with a selected energy of 88 keV, allowed investigations of bulk samples because the absorption length is approximately 2.2 mm for Ce_2Fe_{17}, larger than the thickness of either the polycrystalline or single-crystal samples. The beam size was 500×500 μm^2 limited by a rectangular slit system. For the high-energy x-ray measurements of both the powder and single-crystal samples, the full two-dimensional diffraction patterns were recorded using a MAR345 image-plate system positioned 730 mm behind the sample. The active detection area of 3450×3450 pixels of size 100×100 μm^2 covered a total scattering angle 2θ of 13°, or a reciprocal space range of 12 $Å^{-1}$ at this energy.

III. MEASUREMENTS AND RESULTS

A. Laboratory x-ray measurements of a single crystal

In the preliminary diffraction study of a Ce_2Fe_{17} single crystal on a standard four-circle diffractometer, strong reflections were found at positions (H K L) in hexagonal notation with $-H+K+L=3n$, where H, K, L, and n are integers according to the space group $R\bar{3}m$ for the known room-temperature crystal structure. In what follows, we categorize these reflections as the main reflections. Below T_t, additional reflections were systematically observed at positions (H K $L+3/2$), as shown in Fig. 1. Even though these additional reflections are weak, they indicate an enlarged unit cell or crystallographic superstructure. Hence, these reflections

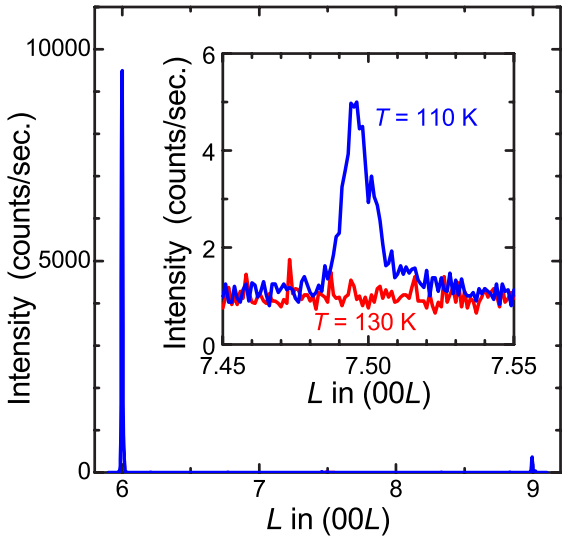

FIG. 1. (Color online) Diffraction patterns of the Ce_2Fe_{17} single crystal measured using Cu $K\alpha$ x rays at $T=110$ and 130 K, well below and above the crystallographic phase transition, respectively. Parts of the patterns around the (0 0 15/2) position are enlarged in the inset.

are categorized as superstructure reflections. Their measured intensity is nearly 4 orders of magnitude lower than that of the main reflections, as illustrated in Fig. 1. The transverse peak widths of both sets of reflections (rocking curves), however, are similar (0.03°). While these measurements clearly establish the existence of a crystallographic superstructure in Ce_2Fe_{17} below T_t, elucidation of the nature of the modified unit cell requires a more extensive study of the superstructure diffraction peaks.

B. High-energy x-ray diffraction measurements of a powder sample

In an attempt to collect additional superstructure peaks associated with the modified chemical unit cell below T_t, diffraction patterns of the polycrystalline Ce_2Fe_{17} sample were measured at different temperatures between $T=10$ and 300 K using the high-energy x rays available in Station 6ID-D of the MUCAT sector at the Advanced Photon Source. For the polycrystalline sample, the data were integrated over the Debye-Scherrer cone, collected by the area detector, to obtain the diffracted intensity as a function of the scattering angle 2θ. Additionally, the sample was continuously rocked around its vertical axis up to ±2.9°. An adequate averaging over sample grains was thus achieved.

Figure 2 shows patterns measured at base temperature, $T=10$ K, and at 130 K, which is slightly above the transition temperature T_t. The lower panel shows the difference between the two diffraction patterns. The difference is dominated by the decrease of the intensity of Bragg reflections with increasing temperature due to thermal motion. Additionally, the thermal lattice expansion yields small shifts of the reflections, yielding differences in the patterns. Besides these effects, the diffraction patterns remain essentially the

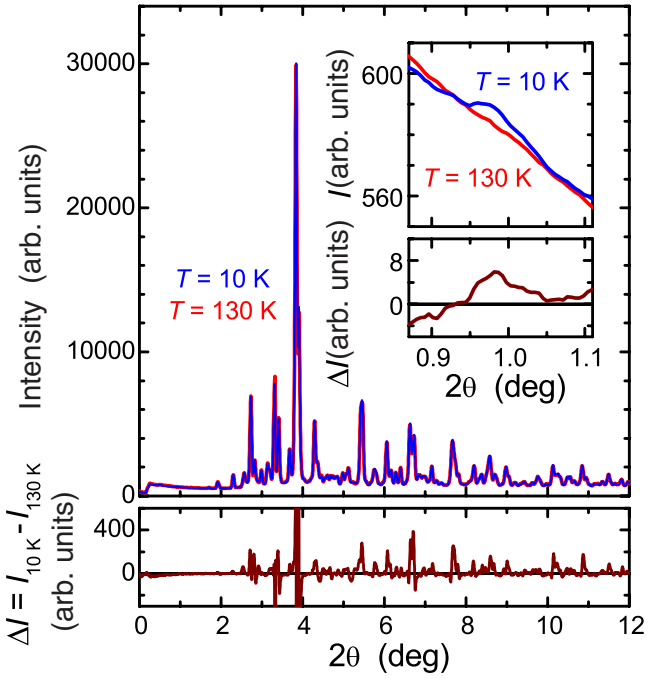

FIG. 2. (Color online) High-energy x-ray diffraction patterns of Ce_2Fe_{17} powder measured with $\lambda = 0.141$ Å. The upper panel shows diffraction patterns at $T = 10$ and at 130 K. The difference between the intensities at both temperatures is shown in the lower panel. Parts of the patterns around the (0 0 3/2) position are enlarged in the inset.

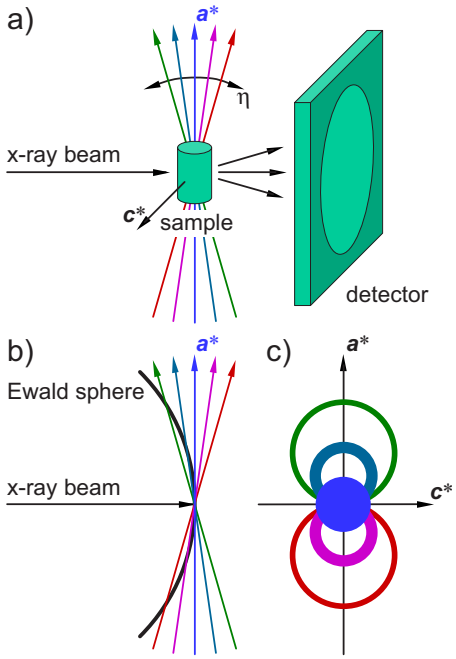

FIG. 3. (Color online) Special rocking technique to measure entire reciprocal planes of a Ce_2Fe_{17} single crystal using high-energy x rays. Here, it is illustrated for the recording of the (H 0 L) plane. Dimensions and angles are not to scale and, partly, strongly exaggerated for a better illustration. (a) Instrumental geometry with the image-plate detector mounted centered and perpendicular to the incident x-ray beam behind the sample. The direct x-ray beam is blocked by a small beam catcher not shown here. Tilting by the angle η is visualized by the resulting fan of the $\mathbf{a}^*$ direction. (b) Ewald illustration of the scattering geometry in reciprocal space. The tilting of the reciprocal lattice caused by the sample tilting is visualized by the fan of the $\mathbf{a}^*$ direction. (c) View onto the reciprocal (H 0 L) plane in beam direction. The circle and the annuli represent the intersection between the Ewald sphere and the (H 0 L) plane for the different tilting angles η shown in (a) and (b).

same. Therefore, the main features of the crystallographic structure are unchanged between $T = 10$ and 130 K.

Below T_t, however, a very weak additional reflection was observed at low scattering angles 2θ. The inset in Fig. 2 shows this reflection which can be indexed as (0 0 3/2). Its intensity increases with decreasing temperature, and it is about 4 orders of magnitude lower than the strongest reflections at room temperature, consistent with the superstructure observed in the laboratory measurements described above. Unfortunately, observations of related superlattice reflections at higher scattering angles 2θ failed due to the overlap with much stronger reflections corresponding to the room-temperature crystal structure.

C. High-energy x-ray diffraction measurements of a single crystal

In order to unambiguously determine the nature of the superstructure below T_t in Ce_2Fe_{17}, measurements of single crystals over a wide range of reciprocal space are required. For the single crystal, a special rocking technique was applied to record the diffraction intensity within planes in reciprocal space. The scattering geometry of Fig. 3 describes the experiment. In Fig. 3(b), the scattering geometry is represented by an Ewald sphere fixed in the coordinate system of the instrument. The image plate records all points on the Ewald sphere, up to the maximum scattering angle 2θ given by the ratio of the dimension of the image plate and the distance between sample and detector. The origin of reciprocal lattice is located at the center of the recorded pattern. The orientation of the reciprocal lattice relative to the Ewald sphere is given by the orientation of the sample in the instrument [Fig. 3(a)]. It can be modified by two independent tilting angles perpendicular to the incoming beam. If the designated reciprocal plane is perpendicular to the incident beam, only one point, the origin, is intersected by the Ewald sphere. If the sample is now tilted by a small angle, the intersection between the Ewald sphere and the designated reciprocal plane is a circle and can be recorded. The diameter of this circle increases with increasing tilting angle. In any experimental measurement, the resolution is finite, and, consequently, an annulus is recorded as illustrated in Fig. 3(c). By tilting the sample through both angles and summing the recorded patterns, an extended piece of the designated reciprocal plane can be recorded. To obtain the entire reciprocal plane without gaps, both tilting angles have to be scanned in a two-dimensional mesh, and the step size for the sampling mesh has to be adjusted to the instrumental resolution and the mosaic spread of the sample.

Unfortunately, points away from the designated reciprocal plane are also recorded. Depending on the dimensions of the

reciprocal lattice and the tilting angles, reciprocal planes other than the designated plane will also intersect the Ewald sphere. This limits the analyzable area of the recorded pattern and, accordingly, the maximum range of meaningful tilting angles. The diameter of the analyzable area is proportional to the radius of the Ewald sphere given by the length of the wave vector of the incident x rays. The use of high-energy x rays significantly enhances this study because the relatively short wavelength corresponds to a large magnitude of the incident wave vector. A considerable amount of time was required to read out the image plate. Therefore, the image plate was exposed during the full time of meshing both tilting angles rather than recording separate patterns at stepwise increments in the tilting angles. An additional advantage of this method is the opportunity to scan one tilting angle continuously, as only the second tilting angle needs to be changed stepwise.

The study of the Ce_2Fe_{17} single crystal was performed by scanning the horizontal angle φ up to ±1.8° and stepping the vertical angle η up to ±1.8° with a step size of 0.15°. The total exposure time was 150 s. for each pattern, which was determined by the maximum motor speed for the tilting angles. Aluminum attenuators were used to adapt the scattered intensity to the dynamic range of the image-plate system. Furthermore, to eliminate extraneous reflections from the Be domes as discussed above, an aluminum enclosure with Kapton windows was used for these measurements. In Fig. 4, diffraction patterns are shown for the three most relevant reciprocal planes $(H\ H\ L)$, $(H\ K\ 0)$, and $(H\ 0\ L)$. In Figs. 4(a) and 4(b), the left part of the pattern should be identical to the flipped one from the right part as a consequence of the mirror planes perpendicular to the shown reciprocal plane according to the space group $R\bar{3}m$. In contrast, no mirror plane is present in the $(H\ 0\ L)$ plane shown in Fig. 4(c). However, the twofold rotation axis perpendicular to this plane should yield an identical diffraction pattern after a rotation by 180°.

Above T_t, the diffraction patterns were consistent with the room-temperature crystal structure. Weak ringlike scattering features in the patterns arose from small amounts of polycrystalline $CeFe_2$ and an undefined polycrystalline sample impurity. In the $(H\ 0\ L)$ plane, reflections were observed at positions $(H\ 0\ L)$ with $-H+L=3n$, where H, L, and n are integers, according to the space group $R\bar{3}m$. Interestingly, no reflections were found at positions $(H\ 0\ L)$ with $H+L=3n$, where H, L, and n are integers, expected for a twinned single crystal. Below T_t, superstructure reflections were observed in the $(H\ 0\ L)$ and $(H\ H\ L)$ planes at positions displaced by $(0\ 0\ 3/2)$ from positions related to the room-temperature crystal structure. No other extra reflections were observed. In the $(H\ K\ 0)$ plane, no superstructure reflections were found. All diffraction patterns measured at low temperatures are consistent with a unit cell doubled along the c direction based on the dimensions of the room-temperature unit cell.

To measure the temperature dependence of the superstructure reflections, diffraction patterns of the $(H\ 0\ L)$ plane were recorded, but with the sample enclosed by the beryllium domes. The reflection intensity I was determined as function of the well-defined sample temperature T by fitting two-dimensional Gaussian-shaped peaks to the diffraction patterns. Figure 5 shows the result for selected superstructure reflections. The good agreement between the intensity of the corresponding Friedel-pair reflections indicates a properly

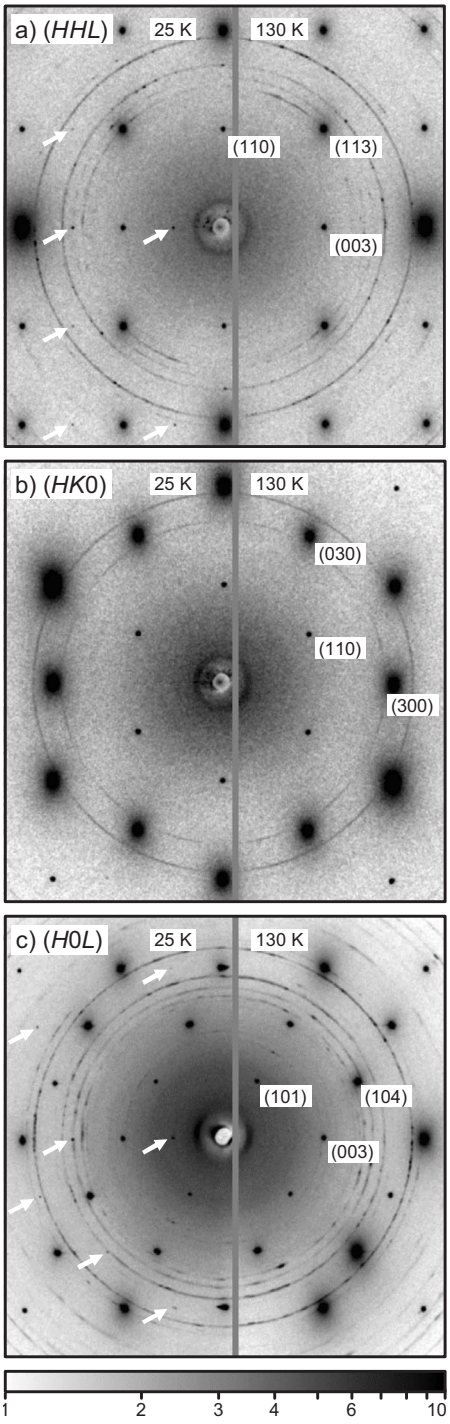

FIG. 4. High-energy x-ray diffraction patterns of the Ce_2Fe_{17} single crystal. The intensity is encoded by the gray tone in the contour map of the (a) $(H\ H\ L)$, (b) $(H\ K\ 0)$, and (c) $(H\ 0\ L)$ planes. The left and right sides show measurements at $T=25$ and at 130 K, respectively, which is above the crystallographic phase transition. The arrows point to superstructure reflections appearing in the low-temperature phase.

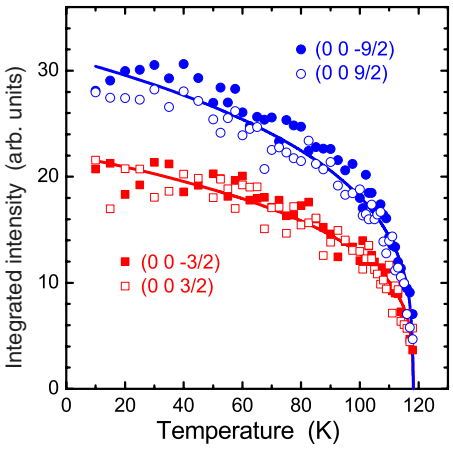

FIG. 5. (Color online) Temperature (T) dependence of the integrated intensity (I) of superstructure reflections measured with high-energy x rays on the Ce_2Fe_{17} single crystal. The lines represent power-law curves describing the combined data for the Friedel-pair reflections $(0\ 0 \pm 3/2)$ and $(0\ 0\ \pm 9/2)$, respectively.

chosen experimental geometry. The temperature-dependent data are well described by a power law. A transition temperature $T_t = 118 \pm 2$ K was consistently determined for all investigated reflections. This transition temperature is consistent with that observed in low-field magnetization measurements of the same sample. The transition temperature is slightly lower than for the samples in Ref. 7. The difference is likely caused by a small amount of a dopant. Recently, for example, we have found that a doping by only 0.1% of Al for Fe causes a decrease in T_t by about 10 K.[19]

IV. DISCUSSION

A. Superstructure and crystallographic phase transition

In Ce_2Fe_{17}, a crystallographic superstructure was found below $T_t = 118 \pm 2$ K. In addition to the measurements described here, we have observed similar crystallographic superstructure reflections in recent neutron diffraction experiments as well as in x-ray resonant magnetic scattering (XRMS) studies, which will be presented elsewhere. However, it is worth emphasizing here that the sample penetration depth for all of these structural probes covers a large range from ~ 2 μm in the XRMS study at the Ce-L_2 absorption edge to 2.2 mm for the high-energy x-ray diffraction experiments, and up to a few centimeters for the scattering of thermal neutrons, respectively. Thus, these experiments have probed the formation of the superstructure in different parts of the sample, from near-surface regions through the entire bulk. In all cases, the widths of the superstructure reflections were similar to the widths of the main reflections. This indicates that the superstructure forms with the same degree of perfection as the main crystal structure in every part of the sample. The intensity ratio between the superstructure and main reflections was consistent in all these studies. From these results, it can be concluded that the superstructure is uniform throughout the entire Ce_2Fe_{17} sample.

We now turn to a discussion of the space group of the low-temperature superstructure as determined by an analysis of possible crystallographic subgroups of the room-temperature space group $R\bar{3}m$. The observed doubling of the unit cell in the hexagonal c direction corresponds to a doubling of the length along the body diagonal in the rhombohedral lattice. Only two subgroups of the space group $R\bar{3}m$ are related to a doubling of the unit cell in the **c** direction, the nonisomorphic subgroup (A) $R\bar{3}c$ ($\mathbf{a}' = -\mathbf{a}$, $\mathbf{b}' = -\mathbf{b}$, $\mathbf{c}' = 2\mathbf{c}$) and the isomorphic subgroups (B) $R\bar{3}m$ ($\mathbf{a}' = -\mathbf{a}$, $\mathbf{b}' = -\mathbf{b}$, $\mathbf{c}' = 2\mathbf{c}$).[20] The prime symbol ($'$) denotes the subgroup. Both subgroups (A) and (B) yield a general condition for $(H'\ K'\ L')$ reflections with $-H' + K' + L' = 3n$, which can be satisfied by the observed diffraction patterns considering the transformation $L'/2 = L$. The subgroup (A) $R\bar{3}c$ contains an additional general condition for $(H'\ -H'\ L')$ reflections with $H' + L' = 3n$ and $L' = 2n$ caused by the glide plane.[20] However, the observed reflections violate this condition, e.g., reflections were present at (0 0 3/2) and (0 0 9/2) positions which would be (0 0 3) and (0 0 9), respectively, in the notation of the subgroup. As result, only subgroup (B) is possible. All observed diffraction patterns are in agreement with this subgroup, with $R\bar{3}m$ ($\mathbf{a}' = -\mathbf{a}$, $\mathbf{b}' = -\mathbf{b}$, $\mathbf{c}' = 2\mathbf{c}$) as space group for the low-temperature phase.

The doubling of the unit cell in **c** relates to a substitution of the symmetry element translation with the vector **c** by a translation with the vector 2**c**, which corresponds to a twofold reduction of the symmetry. Therefore, the transition from the room-temperature structure to the low-temperature superstructure can be described by a transition to a direct subgroup of the original space group of index 2.[20]

Table I lists the transformation of the atomic positions and their Wyckoff sites according to the subgroup description defined above. For atoms on the original Wyckoff sites 6c, 18f, and 18h, the site symmetry is not changed by the phase transition. Consequently, these sites split up into two new sites with a doubling of the number of free parameters for the atomic positions according to the index 2 of the subgroup. The situation is different for the original Wyckoff site 9d which transforms to the new Wyckoff site 18h. The new site symmetry m is, by index 2, lower than the original site symmetry $2/m$. The missing symmetry element yields two new free parameters for the new Wyckoff position $(x, -x, z)$ in contrast to the fixed original Wyckoff position $(1/2, 0, 1/2)$,[20] see Table I.

The observed intensity of superstructure reflections can be used for an order-of-magnitude estimate of the corresponding displacement of atoms from their room-temperature position with higher symmetry. The observed intensity ratio between the superstructure reflection (0 0 15/2) at $T = 110$ K and the main reflection (0 0 6) at $T = 130$ K, respectively, is roughly 4:9500 as shown in Fig. 1. This intensity ratio depends only on the z position of the atoms because (0 0 L) reflections average structure features perpendicular to the z direction. Two different cases of atomic displacements are considered. In the first, the superstructure is caused by a displacement of only one atomic site, the Fe site 6c, for example. A displacement of ± 0.005 unit cell lengths along the z direction is required to obtain the observed intensity ratio. In a second scenario, all atoms are displaced in the z

TABLE I. Wyckoff sites and atomic coordinates for the room-temperature phase in Ce_2Fe_{17} and their transformation into the low-temperature phase. The symbols x, y, z and decimal-point numbers represent free parameters. The space group is $R\bar{3}m$ for both phases. The lattice parameters transform according to $\mathbf{a}_{\text{low } T} = -\mathbf{a}_{\text{room } T}$, $\mathbf{b}_{\text{low } T} = -\mathbf{b}_{\text{room } T}$, and $\mathbf{c}_{\text{low } T} = 2\mathbf{c}_{\text{room } T}$.

		Room T				Low T		
		x	y	z		x	y	z
Ce	6c	0	0	z	6c	0	0	$z/2$
					6c	0	0	$z/2+1/2$
Fe	6c	0	0	z	6c	0	0	$z/2$
					6c	0	0	$z/2+1/2$
Fe	9d	1/2	0	1/2	18h	0.5	−0.5	0.25
Fe	18f	x	0	0	18f	$-x$	0	0
					18g	$-x$	0	1/2
Fe	18h	x	$-x$	z	18h	$-x$	x	$z/2$
					18h	$-x$	x	$z/2+1/2$

direction by an equal distance. The sense of direction for the displacement is chosen in such a manner that the intensity ratio is maximized. The result is a displacement of ±0.002 unit cell lengths. These two cases represent roughly the upper and lower limits for atomic displacements related to the observed superstructure. These very slight changes in the crystal structure are consistent with the observed marginal changes of the main reflections.

According to Landau's theory, a phase transition described by a subgroup relation is consistent with a second order phase transition where a symmetry element is broken and an order parameter starts to develop.[21] The atomic displacement must follow the temperature dependence of the intensity, because the intensity of superstructure reflections depends quadratically on the value of the atomic displacement. Hence, the atomic displacement can be considered as the order parameter of this phase transition. It starts at the transition temperature without a jump. Therefore, no abrupt rearrangement of atoms is necessary to originate the observed behavior around the phase transition. It can be described as a diffusionless movement of atoms consistent with a second order phase transition.

B. Influence of the crystallographic phase transition on magnetic and electronic properties

As discussed in the Introduction, the magnetic properties of Ce_2Fe_{17} seem particularly sensitive to small changes in chemistry and structure. The magnetic and electronic properties can be influenced in several manners by the observed crystallographic phase transition. We now consider the effect of the change in local symmetries and of the additional freedom in atomic positions as well as the consequences of the doubling of the unit cell.

A lowering of the site symmetry is associated with a lowering of the symmetry of the crystal electric field for the atoms on this site. However, only minor changes in the magnetocrystalline anisotropy are expected because the crystal electric field effects are less important in Ce_2Fe_{17}. More relevant for the magnetism is the splitting of the original single Wyckoff sites into pairs of Wyckoff sites. The related doubling of the number of free parameters for the atomic positions yields changes in the distance and angle between magnetic neighbor atoms which can, in principle, affect the strength of the magnetic exchange.[22,23] This can be important for Ce_2Fe_{17} in light of the delicate balance between antiferromagnetic and ferromagnetic interactions. For example, for the Fe atoms originally located on the Wyckoff site 9d, the effect is not only quantitative, but it is also qualitative due to the change in the local symmetry at the phase transition. For the room-temperature structure, these atoms are located on a twofold rotation axis. Thus, neighbor atoms are pairwise symmetry coupled, and the distances between them are equal. This condition is lost in the low-temperature structure, and the distances between these neighboring atoms are different. Consequently, the strength of the magnetic exchange between these neighboring atoms is no longer equal, possibly leading, in some cases, to a change in sign of the magnetic exchange.

In the low-temperature phase, the doubling of the unit cell along the hexagonal **c** direction in real space halves the Brillouin zone in the $\mathbf{c}^*$ direction, and the shape of the Brillouin zone changes accordingly, because the dimension in the $\mathbf{c}^*$ direction is now much smaller than in other directions. This is evidenced in Fig. 4 by the smaller distances along the $\mathbf{c}^*$ direction between reflections, normal and superstructure reflections together, in comparison to other directions. Modifications of the electronic band structure, associated with the opening of a new superzone gap, can be expected and can result in changes in the transport properties. Indeed, in measurements of the electric conductivity on Ce_2Fe_{17} single crystals, a strong increase in resistivity was observed below the transition temperature T_t.[7] This increase is strongly anisotropic; it is much larger for the current flowing parallel to

the **c** direction than for the current flowing perpendicular to the **c** direction. A detailed description of this effect consistent with the formation of anisotropic superzone gaps is given in Ref. 7. It should be mentioned that the crystallographic phase transition occurs in the antiferromagnetically ordered state with an incommensurate propagation vector in the $\mathbf{c}^*$ direction. Both superstructures, the crystallographic superstructure and the antiferromagnetic superstructure, can yield superzone gaps and, therefore, can cause the change in resistivity at the phase transition temperature T_t. In break-junction measurements, the differential conductance exhibits gap features associated with the low-temperature phase below T_t.[24] Remarkably, features were determined at two energy scales, 12–14 and 26–32 meV, on a polycrystalline sample at $T=4.2$ K. This could be related to the existence of two different gap features probably caused by the changes in the crystal structure and in the magnetic order.

In addition to generating superlattice reflections, the change in the chemical unit cell below T_t also modifies the description of the magnetic order in reciprocal space and, accordingly, the pattern for magnetic scattering. In neutron powder experiments, satellite reflections related to the antiferromagnetic structure with an incommensurate propagation vector in the hexagonal $\mathbf{c}^*$ direction were observed below T_N.[16–18] Below T_t, additional satellite reflections were observed, which could be indexed with the same propagation vector, but starting from the reference position (0 0 3/2). The crystal superstructure determined in this paper yields new lattice points at just such positions. Therefore, the results of the earlier neutron scattering experiments[16–18] can be reinterpreted as the observation of magnetic satellite reflections according to the same incommensurate propagation vector based on the lattice of the new superstructure. Accordingly, the number of pairs of observed antiferromagnetic satellite reflections is doubled below T_t in comparison to the number above T_t.

Based on these results, additional information can now be extracted from the neutron powder diffraction patterns of Ce_2Fe_{17} measured under isotropic pressures up to 5 kbar.[6,13,14] At ambient pressure, a ferromagnetic state was observed in this sample related to a different sample preparation (see Ref. 7). An antiferromagnetic state can be induced by pressures higher than 3 kbar at $T=40$ K.[6] Two groups of antiferromagnetic satellite reflections appear. The first group consists of satellite reflections related to an incommensurate propagation vector similar to those observed for antiferromagnetic order at higher temperatures at ambient pressure. The second group of reflections were indexed with a new, different incommensurate propagation vector.[6] However, these new satellite reflections at $2\theta \sim 11°$. shown in Fig. 11 of Ref. 6 can be indexed by $(0\ 0\ 3/2)^-$. All new satellite reflections can be indexed in the same way as the low-temperature antiferromagnetic phase discussed in the present work. This reinterpretation is supported by the pressure dependence of the positions of these reflections; the $(0\ 0\ 3/2)^-$ reflection moves in the opposite direction to the $(0\ 0\ 0)^+$ reflection. This suggests that the ferromagnetic-antiferromagnetic phase transition at a pressure of 3 kbar is connected with the appearance of a similar superstructure as observed in Ce_2Fe_{17} samples, which show an antiferromagnetic state at low temperatures at ambient pressure.

V. CONCLUSIONS

In conclusion, a superstructure was observed in Ce_2Fe_{17}, which appears below $T_t=118\pm2$ K in the antiferromagnetically ordered state. It can be described by a doubling of the unit cell in the hexagonal **c** direction and the same space group $R\bar{3}m$ as the room-temperature structure. The second order phase transition is realized by a diffusionless movement of atoms. The additional freedom in atomic positions and the change in local symmetry for the Fe atoms at the original Wyckoff sites 9*d* can influence the magnetic behavior due to the delicate balance between antiferromagnetic and ferromagnetic interactions, which are strongly dependent on the distance between neighboring Fe atoms. The halving of the Brillouin zone in the $\mathbf{c}^*$ direction can cause a superzone gap in the electronic structure, which is consistent with the observation of an anisotropic increase in the electric resistivity below T_t. Additional antiferromagnetic satellite reflections observed in former neutron diffraction experiments can be conclusively related to the appearance of the crystallographic superstructure, independent of the ground state of the sample.

ACKNOWLEDGMENTS

The authors thank J. Frederick and S. Jia for the assistance in sample preparation. We are indebted to D. S. Robinson for his excellent support of our experiments. Work at the Ames Laboratory was supported by the Department of Energy, Basic Energy Sciences (or appropriate sponsor), under Contract No. DE-AC02-07CH11358. Use of the Advanced Photon Source (APS) was supported by the U.S. Department of Energy, Basic Energy Sciences, under Contract No. DE-AC02-06CH11357. The Midwest Universities Collaborative Access Team (MUCAT) sector at the APS is supported by the U.S. Department of Energy, Basic Energy Sciences, through the Ames Laboratory under Contract No. DE-AC02-07CH11358.

*Also at Institut für Festkörperphysik, Technische Universität Dresden, D-01062 Dresden, Germany; kreyssig@ameslab.gov

[1] K. J. H. Buschow, Rep. Prog. Phys. **40**, 1179 (1977).
[2] J. M. D. Coey, J. E. M. Allan, A. A. Minakov, and Yu. V. Bugaslavsky, J. Appl. Phys. **73**, 5430 (1993).
[3] Y. Makihara, H. Fujii, T. Fujiwara, K. Watanabe, K. Takahashi, K. Koyama, and M. Motokawa, Physica B **329-333**, 663 (2003).
[4] Y. Janssen, H. Fujii, T. Ekino, K. Izawa, T. Suzuki, T. Fujita, and F. R. de Boer, Phys. Rev. B **56**, 13716 (1997).
[5] A. G. Kuchin, A. N. Pirogov, V. I. Khrabrov, A. E. Teplykh, A. S.

Ermolenko, and E. V. Belozerov, J. Alloys Compd. **313**, 7 (2000).
[6] O. Prokhnenko, C. Ritter, Z. Arnold, O. Isnard, J. Kamarád, A. Pirogov, A. Teplykh, and A. Kuchin, J. Appl. Phys. **92**, 385 (2002).
[7] Y. Janssen, S. Chang, A. Kreyssig, A. Kracher, Y. Mozharivskyj, S. Misra, and P. C. Canfield, preceding paper, Phys. Rev. B **76**, 054420 (2007).
[8] M. Artigas, D. Fruchart, O. Isnard, S. Miraglia, and J. L. Soubeyroux, J. Alloys Compd. **270**, 28 (1998).
[9] A. G. Kuchin, V. I. Khrabrov, A. S. Ermolenko, E. V. Belozerov, and G. M. Makarova, Phys. Met. Metallogr. **90**, 123 (2000).
[10] A. N. Pirogov, A. E. Teplykh, A. G. Kuchin, and E. V. Belozerov, Phys. Met. Metallogr. **90**, 186 (2000).
[11] D. Hautot, G. J. Long, F. Grandjean, and O. Isnard, Phys. Rev. B **62**, 11731 (2000).
[12] S. R. Mishra, G. J. Long, O. A. Pringle, D. P. Middleton, Z. Hu, W. B. Yelon, F. Grandjean, and K. H. Buschow, J. Appl. Phys. **79**, 3145 (1996).
[13] O. Prokhnenko, C. Ritter, Z. Arnold, O. Isnard, A. Teplykh, J. Kamarád, A. Pirogov, and A. Kuchin, Appl. Phys. A: Mater. Sci. Process. **74**, S610 (2002).
[14] O. Prokhnenko, I. Goncharenko, Z. Arnold, and J. Kamarád, Physica B **350**, 63 (2004).
[15] A. V. Andreev and A. Lindbaum, J. Alloys Compd. **297**, 43 (2000).
[16] R. Plumier and M. Sougi, *Proceedings of the International Conference on Magnetism 1973* (Nauka, Moscow, 1974), Vol. 3, p. 487.
[17] H. Fukuda, Y. Janssen, H. Fujii, T. Ekino, and Y. Morii, JAERI-Review **99-007**, 94 (1999).
[18] H. Fukuda, Y. Janssen, H. Fujii, T. Ekino, and Y. Morii, J. Magn. Soc. Jpn. **23**, 108 (1999).
[19] Y. Janssen *et al.* (unpublished).
[20] *International Tables for Crystallography*, edited by T. Hahn (Kluwer Academic, Dordrecht, 1996), Vol. A.
[21] L. D. Landau, Zh. Eksp. Teor. Fiz. **7**, 19 (1937).
[22] R. Coehoorn, Phys. Rev. B **39**, 13072 (1989).
[23] D. Givord and R. Lemaire, IEEE Trans. Magn. **MAG-10**, 109 (1974).
[24] T. Ekino, H. Umeda, H. Fukuda, Y. Janssen, and H. Fujii, J. Magn. Soc. Jpn. **23**, 111 (1999).